MINISTRY OF EDUCATION AND TRAINING
HCMC UNIVERSITY OF TECHNOLOGY AND EDUCATION

TRUONG QUANG PHUC

RECONFIGURABLE INTELLIGENT SURFACES ASSISTED WIRELESS COMMUNICATION NETWORKS

Major: Electronic Engineering
Major code: 9520203

SUMMARY OF PH.D. THESIS

HO CHI MINH CITY –2025

This thesis was completed at HCMC University of Technology and Education

Supervisor 1: Assoc. Prof. Phan Van Ca
Supervisor 2: Prof. Duong Quang Trung

Reviewer 1:
Reviewer 2:
Reviewer 3:

The dissertation was presented at the primary committee of at Faculty of Electrical and Electronics Engineering, HCMC University of Technology and Education, 2025

LIST OF PUBLICATIONS

*(C1) The paper was presented at the **INISCOM 2022** conference and published in **the Springer LNICST Book Series (Q4).***

P.Q. Truong, V.-C. Phan. (2022). Reconfigurable Intelligent Surfaces for Downlink Cellular Networks. In Industrial Networks and Intelligent Systems. INISCOM 2022. Lecture Notes of the Institute for Computer Sciences, Social Informatics and Telecommunications Engineering, vol 444. Springer, Cham. https://doi.org/10.1007/978-3-031-08878-0_2

*(J1) The paper was published in **the EAI Endorsed Transactions on Industrial Networks and Intelligent Systems**, ranked **Q3** according to **Scopus**.*

P. Q. Truong, T. Do-Duy, V.-C. Phan and A. Masaracchia, "Jointly power allocation and phase shift optimization for RIS empowered downlink cellular networks," EAI Endorsed Transactions on Industrial Networks and Intelligent Systems, vol. 10, no. 4, 2023, http://dx.doi.org/10.4108/eetinis.v10i4.4359

*(J2) The paper was published in the **IEEE Access** journal, ranked **Q1 (SCIE)**.*

P. Q. Truong, T. Do-Duy, A. Masaracchia, N.-S. Vo, V.-C. Phan, D.-B. Ha và T. Q. Duong, "Computation Offloading and Resource Allocation Optimization for Mobile Edge Computing-Aided UAV-RIS Communications," IEEE Access, tập 12, pp. 107971 - 107983, 2024.

CHAPTER 1 OVERVIEW

1.1 Introduction

The development of wireless communication technology has progressed through various generations, from 1G, 2G, 3G, to 4G mobile communication systems. This evolution continues with the ongoing refinement and commercialization of 5G technology in several countries worldwide. The 5G mobile communication system serves as a key enabler for unlocking the potential of the IoT, meeting stringent requirements for speed, bandwidth, and the capacity to support a vast number of users. Evidently, the number of users and devices in IoT networks continues to grow rapidly. According to a Cisco report from February 2019, the number of connected devices could reach 28.5 billion by 2022 [1].

The radio environment is defined as a set of objects that significantly alter the propagation of electromagnetic waves between communication devices [2]. These alterations in electromagnetic wave propagation may manifest as attenuation or scattering, but such changes are generally unpredictable and uncontrollable, except in simplified or idealized scenarios. The inability to control the transmission environment substantially reduces the efficiency of communication. Signal attenuation limits the coverage radius between nodes in the network, while multipath effects degrade the quality and power of the received signal. Notably, signal attenuation is a critical issue to consider when deploying mmWave communication. Consequently, investigating the impact of the wireless transmission environment to modify its characteristics in a manner that enhances system performance is a significant research concern [3] [4].

In cooperative wireless communication networks, to enhance performance, DF and AF techniques are employed to process received signals. In the AF technique, relays amplify the received signal before retransmitting an amplified version [5]. However, while the AF technique is relatively simple to implement, it amplifies both the desired signal and the inherent noise at the relay, which is then forwarded. Additionally, both AF and DF techniques actively process signals, inevitably leading to energy consumption when evaluating the overall system performance. Recent studies have primarily focused on examining and proposing solutions to address the limitations encountered in the practical deployment of communication systems. Additionally, research on intelligent radio environments utilizing RIS or configurable reflective surfaces has garnered significant attention. These studies explore models that offer

numerous advantages compared to conventional radio environments and traditional AF or DF techniques.

1.2 Research Objectives

The objectives of the dissertation focus on the following key research areas:

- Develop a mathematical model for a wireless communication system supported by RIS and evaluate the effectiveness of utilizing RIS in wireless communication systems, such as mobile networks and mobile edge computing systems assisted by UAVs.
- Propose an algorithm to optimize the total network throughput of a SISO mobile communication system supported by RIS.
- Propose an algorithm to minimize total latency and offload computational tasks in a MEC system supported by UAVs and RIS.

1.3 Research Tasks

- Investigate the impact of the radio environment on wireless communication systems and the mathematical models used for analysis, simulation, and application.
- Review and evaluate the current research on RIS.
- Develop a mathematical model for wireless communication systems utilizing RIS, including wave propagation, attenuation, and physical models.
- Evaluate the energy and spectral efficiency of systems incorporating RIS.
- Propose applications of reconfigurable intelligent surfaces in wireless communication systems employing various technologies.
- Study the optimization of power allocation in wireless communication systems using RIS.
- Investigate the optimization of phase shift coefficients for RIS.
- Research the optimization of latency in mobile edge computing systems supported by UAVs and RIS.

1.4 Research Scope and Objectives

Intelligent wireless networks and environments utilizing reconfigurable intelligent surfaces, through the proposal of mathematical models and performance evaluation of the network.

1.5 Research Approach and Methodology

The research approach begins with a comprehensive overview of fundamental issues and the current state of the field, followed by an examination of the proposed application of a novel model through mathematical simulation tools.

The theoretical foundation is established based on a review of relevant scientific publications within the research domain, assessing the current progress and identifying existing challenges. Based on these insights, a suitable mathematical model is proposed for practical systems, and the effectiveness of the proposed model is subsequently evaluated.

1.6 Scientific and Practical Significance of the Research Topic

This dissertation focuses on the application of RIS in wireless communication systems—one of the most pressing and actively researched topics in recent years. The study is highly relevant to the evolution of wireless networks in general, and to the development of 5G and 6G wireless communication systems in particular.

a. Scientific Contribution

A novel RIS-based model is proposed for application in linear communication systems, including cellular mobile networks and MEC systems within UAV-assisted wireless networks. The dissertation proposes and solves the problem of maximizing the total network throughput in RIS-assisted cellular networks, while also analyzing the worst-case user throughput under QoS constraints. Furthermore, it proposes and solves the problem of minimizing the total latency in UAV-assisted wireless networks for MEC systems.

b. Practical Contribution

The proposals studied in this dissertation are fully aligned with current trends in the development and real-world deployment of wireless communication networks, especially in the context of the continuously increasing demand for services and the exponential growth in the number of connected devices. Moreover, the proposed models are highly compatible with the ongoing 5G network deployment initiatives led by the Ministry of Information and Communications, as well as by major domestic telecommunications corporations such as Viettel and VNPT.

CHAPTER 2 THEORETICAL FOUNDATIONS

This chapter presents the theoretical foundations of RIS, including RIS-assisted wireless channel models and the applications of RIS in 6G wireless communication networks. In addition, it covers the theoretical background of UAV-assisted wireless communication systems and MEC systems. The chapter also discusses key performance metrics in 6G wireless networks and various optimization techniques for enhancing network performance.

CHAPTER 3 THROUGHPUT OPTIMIZATION IN RECONFIGURABLE INTELLIGENT SURFACE-AIDED CELLULAR NETWORKS

This chapter examines the application of RIS in cellular networks. Specifically, the total network throughput is maximized under the constraints of system power consumption and QoS requirements.

3.1 System Model of IRS-Assisted Cellular Wireless Networks

The downlink model in a SISO cellular network serving multiple users with the support of an RIS is proposed in Figure 3.1. It consists of a single-antenna base station serving $M = \{1, \dots, M\}$ user groups, with a varying number of users in each group, uniformly distributed within the coverage area of the base station.

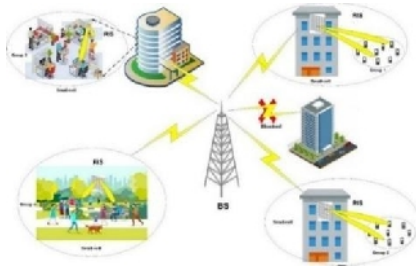

Figure 3. 1 Cellular Network Model with RIS Assistance.

3.1.1 Wireless Transmission Channel and Information Throughput

Consider a coordinate system consisting of the BS and the users: $(x_0, y_0, H_0), (x_m, y_m, H_m), m \in M$ $(x_k, y_k, 0)$, k ∈ K, H_0 and H_m represent the height of the BS and the height at which the RIS is placed, respectively. The communication path from the BS to the user consists of: the channel from the BS to the RIS and the channel from the RIS to the user. The free-space propagation model from the BS to the RIS is given as follows [63], [64]:

$$\beta_{0,m} = \beta_0 R_{0,m}^{-2},\ m = 1, \dots, M, \tag{3.1}$$

In equation (3.1), β_0 is the channel gain considered at the reference position, and $R_{0,m}$ is the distance from the base station to the *m-th* RIS.

$$R_{0,m} = \sqrt{d_{0,m}^2 + (H_0 - H_m)^2}, \tag{3.2}$$

with $d_{0,m} = \sqrt{(x_0 - x_m)^2 + (y_0 - y_m)^2}$.

The reflection path from the RIS to the user (NLoS) [65], the path loss from the *m-th* to the *(m,k)* user is as follows:

$$\begin{aligned} \beta_{m,k} &= PL_{m,k} + \eta^{LoS} P_{m,k}^{LoS} + \eta^{NLoS} P_{m,k}^{NLoS} \\ &= 10\alpha log\left(\sqrt{d_{m,k}^2 + H_{U,m}^2}\right) + AP_{m,k}^{LoS} + B \end{aligned} \tag{3.3}$$

Wherein η^{LoS} và η^{NLoS} are the path loss coefficients for the LoS and NLoS paths, with $A = \eta^{LoS} - \eta^{NLoS}$ and $B = 10\alpha \log\left(\frac{4\pi f_c R_{m,k}}{c}\right) + \eta^{NLoS}$.

The path loss as a function of distance is given by the following expression in equation (3.4):

$$PL_{m,k} = 10 \log\left(\frac{4\pi f_c R_{m,k}}{c}\right)^{\alpha}, \tag{3.4}$$

Where f_c is the carrier frequency in Hz, c is the speed of light in meters per second (m/s), and, $\alpha \geq 2$ is the path loss exponent. The probability of LoS and NLoS [66] is given as follows:

$$P_{m,k}^{LoS} = \frac{1}{1 + a \exp\left[-b\left(\arctan\left(\frac{H_{U,m}}{d_{m,k}}\right) - a\right)\right]}, \tag{3.5}$$

$$P_{m,k}^{NLoS} = 1 - P_{m,k}^{LoS}, \tag{3.6}$$

where a and b are environmental constants.

When the phase shift effect on the RIS $\boldsymbol{\Phi}_m = diag[\phi_{1m}, \phi_{2m}, \ldots, \phi_{Nm}]$. Wherein $\phi_{nm} = \alpha_{nm} e^{j\theta_{nm}}$ with $\alpha_{nm} \in [0,1]$ representing the amplitude and phase angle of the reflected signal at the *n* element of the *m* RIS. It is assumed that the amplitude of the reflected signal is not changed by the RIS elements, so we set $\alpha_{nm} = 1$ [67]. Assuming that the fading in the propagation from the BS to the IRS are independent and identically distributed (i.i.d.) random variables, with $\widehat{h_{0,m}} \in C^{N\times\mathbb{1}}$ and $\widehat{h_{m,k}^H} \in C^{\mathbb{1}\times N}$, where H denotes the Hermitian transpose operator. $\boldsymbol{h}_{0,m} \in C^{N\times\mathbb{1}}$ và $\boldsymbol{h}_{m,k}^H \in C^{\mathbb{1}\times N}$ represent the channel matrices between the BS and the *m-th* RIS and between the *m-th* RIS and the *m-th* user group, respectively. The channel matrix between the BS and the *(m,k)-th* reflected via the *m-th* RIS as follows [68]:

$$\boldsymbol{g}_{m,k} = \boldsymbol{h}_{m,k}^H \boldsymbol{\Phi}_m \boldsymbol{h}_{0,m}, \tag{3.7}$$

In equation (3.7), we have $\boldsymbol{h}_{0,m} = \sqrt{\beta_{0,m}}\widehat{h_{0,m}}$ và $\boldsymbol{h}_{m,k}^H = \sqrt{\beta_{m,k}}\widehat{h_{m,k}^H}$.

Consider the Time Division Multiple Access (TDMA) technique in cellular mobile networks, where the signal is transmitted from the BS to the *m-th* reflecting surface, and the signal is reflected from the reflecting surface to the *m-th* user group. The received signal expression at the user side is given by equation (3.8):

$$y_{m,k} = \sqrt{p_{m,k}}\boldsymbol{g}_{m,k} s_{m,k} + n_k, \tag{3.8}$$

Assume the transmission channel has AWGN, and the BS transmits with power $p_{m,k}$ to the user *(m,k)* and $s_{m,k}$ is the information transmitted from the BS. $\left\|s_{m,k}\right\|^2 \leq 1$; $n_k \sim \mathcal{CN}(0, \sigma_k^2)$ represents the AWGN at the user $(m,k) - th.$ Let $\boldsymbol{p}_0 = \left[\boldsymbol{p}_{0,m}\right]_{m=1}^{M}$, $\boldsymbol{p}_{0,m} = \left[p_{m,k}\right]_{k=1}^{K_m}$,$\boldsymbol{\Phi}_M = [\boldsymbol{\Phi}_m]_{m=1}^{M}$. The SNR expression at the receiver is given by equation (3.9):

$$\gamma_{\mathrm{m,k}}\left(p_{m,k}, \boldsymbol{\Phi}_{\mathrm{m}}\right) = \frac{p_{m,k}\left|\mathbf{g}_{m,k}\right|^2}{\sigma_k^2.} \tag{3.9}$$

3.1.2 Total Network Throughput Optimization Problem

The information throughput of the *k* user in the *m* in *bps/Hz* is given as follows:

$$R_{m,k}\left(p_{m,k}, \boldsymbol{\Phi}_m\right) = \log_2\left(1 + \gamma_{m,k}\left(p_{m,k}, \boldsymbol{\Phi}_m\right)\right). \tag{3.10}$$

The total throughput of all users in the network is given by equation (3.11):

$$R_{total}(p_0, \boldsymbol{\Phi}_M) = \sum_{m=1}^{M}\sum_{k=1}^{K_m} R_{m,k}\left(p_{m,k}, \boldsymbol{\Phi}_m\right). \tag{3.11}$$

The objective in equation (3.12) is to maximize the total system throughput with respect to the transmit power at the BS and the phase shift coefficients of the reflecting elements on the RIS. The constraints considered in equation (3.12) include QoS requirements and maximum transmit power.

$$\max_{p_0, \boldsymbol{\Phi}_M} R_{total}\left(\boldsymbol{p}_0, \boldsymbol{\Phi}_M\right) \tag{3.12a}$$

$$s.t \sum_{m=1}^{M}\sum_{k=1}^{K_{\mathrm{m}}} p_{m,k} \leq P_0^{max}, m \in M, \tag{3.12b}$$

$$R_{m,k}\left(p_{m,k}, \boldsymbol{\Phi}_m\right) \geq \overline{r_{m,k}}, m \in M, k \in K, \tag{3.12c}$$

$$0 \leq \theta_{nm} \leq 2\pi, \forall n = 1, 2, \ldots, N, m \in M, \tag{3.12d}$$

In constraint (3.12b), the total power consumption of all RISs must not exceed the maximum transmit power of the BS, denoted as P_0^{max}. (3.12c) represents the QoS constraint for the *(m, k)-th* user, (3.12d) specifies the upper and lower bounds of the phase shift for the *n-th* reflecting element of the *m-th* RIS.

3.2 Joint Network Sum Throughput Optimization Problem

The optimization problem defined in equation (3.12) is non-convex due to the non-convex nature of functions (3.12a) and (3.12b). Therefore, the power control coefficients at the BS and the phase shifts of the reflecting elements on the RIS are optimized using an iterative approach

3.2.1 Power Allocation Coefficient Optimization at the Base Station

Considering the system with a given phase shift matrix $\boldsymbol{\Phi}_m$, the power control coefficient optimization problem is formulated as in equation (3.13a). Here, the

constraints are as defined in equations (3.12b) and (3.12c), corresponding to the maximum transmit power at the BS and the QoS requirements, respectively.

$$\max_{p_0} \mathrm{R}_{\mathrm{total}}(\boldsymbol{p}_0) \tag{3.13a}$$

$$s.t.\,(3.12b), (3.12c) \tag{3.13b}$$

Based on the approximation and logarithmic inequality transformation method [69], using the concave function $f(z) = \log_2\left(1 + \frac{1}{z}\right) \geq \hat{f}(z)$, we obtain the expression as in equation 3.15:

$$\hat{f}(z) = \log_2\left(1 + \frac{1}{\bar{z}}\right) + \frac{1}{1+\bar{z}} - \frac{z}{(1+\bar{z})\bar{z}}, \tag{3.14}$$

where $\forall z > 0, \bar{z} > 0$, we can rewrite the expression as follows:

$$R_{m,k}(p_{m,k}) \geq \widehat{R_{m,k}^{(\iota)}}(p_{m,k}),\ \forall k \in K_m,\ \forall m \in M, \tag{3.15}$$

$$\widehat{R_{m,k}^{(\iota)}}(p_{m,k}) = \log_2\left(1 + \frac{1}{\bar{z}}\right) + \frac{1}{1+\bar{z}} - \frac{z}{(1+\bar{z})\bar{z}}. \tag{3.16}$$

Then, the optimization problem in equation (3.13) can be reformulated as:

$$\max_{\boldsymbol{p}_0} \widehat{R_{total}^{(\iota)}}(\boldsymbol{p}_0) \tag{3.17a}$$

$$s.t.\,(3.12b) \tag{3.17b}$$

$$\widehat{R_{m,n}^{(\iota)}}(\boldsymbol{p}_0) \geq \overline{r_{m,k}}, m \in M, k \in K, \tag{3.17c}$$

Table 3. 1 Power Control Coefficient Optimization Algorithm

Algorithm 1: Power Allocation

Input:

$i = 0, \boldsymbol{\Phi_M}, \varepsilon = 10^{-3}$

$I_{max} = 20$

Repeat

Solve (3.17) to find $\left(\boldsymbol{p}_0^{(i+1)}\right)$ using CVX.

$i = i + 1$

Until convergence or $i > I_{max}$

Output: $\boldsymbol{p}_0^*$

$\widehat{\boldsymbol{R}_{\boldsymbol{total}}^{(\boldsymbol{\kappa})}}(\boldsymbol{p_0}) = \sum_{\boldsymbol{m=1}}^{\boldsymbol{M}} \sum_{\boldsymbol{k=1}}^{\boldsymbol{K_m}} \widehat{\boldsymbol{R}_{\boldsymbol{m,k}}^{(\boldsymbol{\kappa})}}(\boldsymbol{p}_{\boldsymbol{m,k}})$.

Equation (3.17) is solved using Algo 1 in Table 3.1, with the CVX tool [70]. The values are set as $\boldsymbol{i = 0, \Phi_M}$, và $\boldsymbol{\varepsilon = 10^{-3}}$. The maximum number of iterations is $\boldsymbol{I_{max} = 20}$ and the output of the algorithm is the power control coefficients.

Algorithm 1 is proposed to solve the convex optimization problem in (3.17), maximizing the total achievable rate $R_{total}(p_0)$ with approximately $\mathcal{O}(K)$ variables and $\mathcal{O}(K + N)$ linear constraints Utilizing the convex and continuous nature of the objective function, it ensures fast convergence to the global optimum using the CVX tool, with a stopping criterion of $\varepsilon = 10^{-3}$ or $I_{max} = 20$ iterations and a computational complexity of $\mathcal{O}(K^3)$[84].

3.2.2 Phase Shift Coefficient Optimization for the RIS Reflecting Elements

When the power control coefficient p_0 is considered fixed, the phase shift coefficient optimization problem for the RIS can be described as in equation (3.18), with constraints related to QoS and the phase shift angle limits of the reflecting elements.

$$\max_{\boldsymbol{\Phi}_m} R_{total}(\boldsymbol{\Phi}_m) \tag{3.18a}$$

$$s.t.(3.12c),(3.12d) \tag{3.18b}$$

Let $\boldsymbol{h}_{m,k}^H \boldsymbol{\Phi}_m \boldsymbol{h}_{0,m} = \psi_m^H \chi_{m,k}$ where $\psi_m = [\psi_m^1, \dots, \psi_m^N]^H$ and $\psi_m^n = e^{j\theta_{nm}} (\forall n = 1,2,\dots N)$, $\chi_{m,k} = diag(\boldsymbol{h}_{m,k}^H)\boldsymbol{h}_{0,m}$, and $a_k = P_0/\sigma_k^2$, Considering $|\psi_m^n|^2 = 1$, the expression is as follows:

$$\max_{\psi_m, m\in M} \sum_{m=1}^{M}\sum_{k=1}^{K_m} \log_2\left(1 + a_k \psi_m^H \chi_{m,k} \chi_{m,k}^H \psi_m\right) \tag{3.19a}$$

$$s.t \qquad \psi_m^H \chi_{m,k} \chi_{m,k}^H \psi_m \geq (2^{\overline{r_{m,k}}} - 1)/a_k, \tag{3.19b}$$

$$|\psi_m^n|^2 = 1, \forall n = 1,2,\dots,N, \qquad m \in M \tag{3.19c}$$

However, the above problem is not convex. Let $X_{m,k} = \chi_{m,k}\chi_{m,k}^H$ và $\psi_m^H \boldsymbol{X}_{m,k} \psi_m = tr\left(\boldsymbol{X}_{m,k}\psi_m\psi_m^H\right) = tr\left(\boldsymbol{X}_{m,k}\boldsymbol{\Psi}_m\right)$ where $\boldsymbol{\Psi}_m = \psi_m\psi_m^H$ must satisfy the conditions $\boldsymbol{\Psi}_{\mathrm{m}} \succeq \mathbf{0}$ and $rank(\boldsymbol{\Psi}_{\mathrm{m}}) = 1$.

$$\max_{\psi_m, m\in M} \sum_{m=1}^{M}\sum_{k=1}^{K_m} \log_2\left(1 + a_k tr\left(\boldsymbol{X}_{m,k}\boldsymbol{\Psi}_m\right)\right) \tag{3.20a}$$

$$s.t \qquad tr\left(\boldsymbol{X}_{m,k}\boldsymbol{\Psi}_m\right) \geq (2^{\overline{r_{m,k}}} - 1)/a_k, \tag{3.20b}$$

$$\boldsymbol{\Psi}_{\mathrm{m(n,n)}} = 1, \forall n = 1,2,\dots,N, \qquad m \in M.. \tag{3.20c}$$

$$\boldsymbol{\Psi}_{\mathrm{m}} \succeq \mathbf{0} \tag{3.20d}$$

Table 3. 2 Phase shift Optimization Algorithm

Algorithm 2: Phase shift Optimization

Input:

$\mathrm{i} = 0, \boldsymbol{p}_0, \varepsilon = 10^{-3}$ $I_{max} = 20$

Repeat

for $m = [1:M]$

Solve (3.20) to find $\left(\Phi_M^{(i+1)}\right)$ using CVX.

end for

$$i = i + 1$$

Until convergence or $i > I_{max}$

Output: $\boldsymbol{\Phi}_{\boldsymbol{M}}^*$

The problem in equation (3.20) is solved using Algorithm 2 in Table 3.2, with the CVX tool. The input parameters are set as $\boldsymbol{i = 0, p_0}$, và $\boldsymbol{\varepsilon = 10^{-3}}$. The output of the algorithm is $\boldsymbol{\Phi}_{\boldsymbol{M}}^*$.

Algorithm 2 iteratively solves M subproblems in (3.20), each with approximately $\mathcal{O}(N^2)$ optimization variables and $\mathcal{O}(K_m + N)$ linear constraints, where K_{m} denotes the number of users affected by the *m-th* reflecting element. The overall computational complexity of the algorithm is estimated at approximately $\mathcal{O}(20.M.N^6)$ [84].

3.3 Simulation Results and Discussion

The simulation program was implemented using Matlab software with the support of the CVX library to solve the optimization problem. The simulation parameters were set as shown in Table 3.3. The simulation results were carried out and evaluated for the following cases: **OOP**, **EOP**, **ORP**, **ERP**.

Table 3. 3 Simulation Parameters

No.	Parameter	Value
1.	Number of antennas at the BS	1
2.	Location of the Base Station (BS)	(0, 0, 30) m
3.	Near coverage radius	500m
4.	Far coverage radius	1500m
5.	White noise power spectral density	-130dBm/Hz
6.	QoS threshold	$\varepsilon = 10^{-3}$
7.	Number of RIS reflecting surfaces	[4, 8, 12, 20]
8.	Number of reflecting elements on RIS	[100, 150, 200, 250, 300]
9.	Number of user groups considered	[20, 30]
10	Channel bandwidth	10 MHz
11	Transmit power at the BS	[43:46] dBm

3.3.1. Maximum network throughput

Figure 3.2 shows the evaluation of the network throughput achieved with the transmit power of the BS varying between 43 dBm and 46 dBm, with the number of intelligent RIS reflecting surfaces M =4, the number of user groups K = 20 and a fixed number of reflecting elements N=200. The results indicate that the total network throughput achieved with the support of RIS surfaces is approximately 1.5 times higher when the phase shift coefficients of the reflecting elements are optimized compared to the case where RIS is used without optimizing the phase shift coefficients.

In Figure 3.3, the simulation results are considered for the case where the transmit power at the BS and the number of reflecting elements on the RIS are kept the same as in Figure 3.2. Here, the number of RIS is M=8, and the number of user groups K=30. Compared to the case in Figure 3.2, the total

network throughput increases as the transmit power at the BS increases. Additionally, when the number of RIS reflecting surfaces increases from M = 4 to M = 8, even though the number of users also increases, a significant increase in the total network throughput is observed.

Figure 3.4 shows that increasing the number of reflecting elements on the RIS significantly enhances the network sum throughput across all scenarios. The **OOP** simulation curve demonstrates that the proposed joint optimization method. Figure 3.5 illustrates the network sum throughput of the proposed method when the number of RISs is varied, specifically for M=4, M=12, and M=20. In this case, the network sum throughput increases substantially as the number of RISs increases from 4 to 20. The throughput gap between M=4 and M=20 becomes significantly more pronounced when the transmit power rises from 44 dBm to 46 dBm, corresponding to an improvement of approximately 56 bps/Hz at the maximum transmit power of 46 dBm.

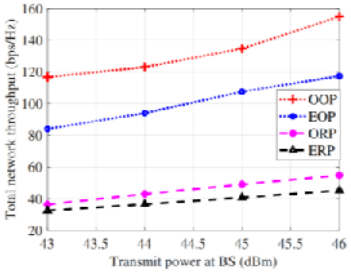

Figure 3. 2 Total Network Throughput M=4, K=20 và N=200

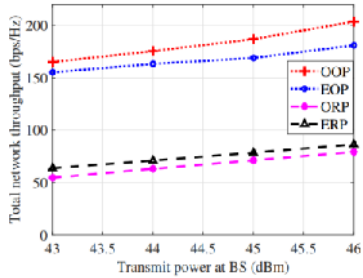

Figure 3. 3 Total Network Throughput M=8, K=30 và N=200

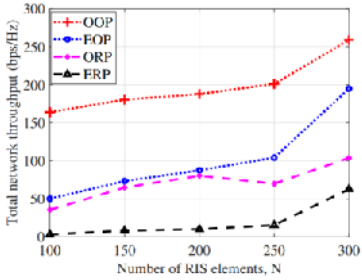

Figure 3.4 Total Network Throughput with N = [100:300], M = 8, K =30, $P_0^{max} = 46\ dBm$

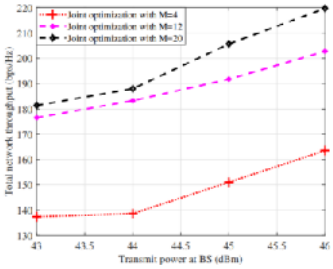

Figure 3. 5 Total Network Throughput with M = 4, M =12, M=20

3.3.2. Worst-Case User Network Throughput

Consider the user throughput (MU) in the worst-case scenario with varying values of the number of users and RIS reflecting elements [71].

The simulation results in Figure 3.6 show that the proposed **OOP** method outperforms **OPH, EOP**, and **ERP**, in the worst-case user throughput with M=8, K=30, and N=200, achieving 1 *bps/Hz* at $P_0^{max} = 43\ dBm$ and doubling at $P_0^{max} = 45\ dBm$ with peak throughput at $P_0^{max} = 46\ dBm$. While **ORP** maintains 1 *bps/Hz* from $P_0^{max} = 43\ dBm$ to $P_0^{max} = 46\ dBm$ and **EOP** reaches approximately 2.5 *bps/Hz* at $P_0^{max} = 45\ dBm$ and $P_0^{max} = 46\ dBm$, **ERP** yields below below 0.5 *bps/Hz*, failing to meet the QoS constraint (3.12c).

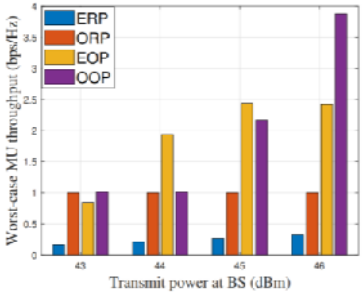

Figure 3. 6 Worst-Case Throughput M = 8, K =30, N = 200.

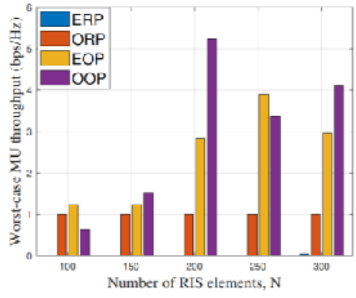

Figure 3. 7 Worst-Case Throughput with N from 100 to 300.

Figure 3.7 illustrates the impact of N on the worst-case user throughput. With $P_0^{max} = 46\ dBm$, M=20, and K=30, while N = [100:300]. The throughput achieved from the worst-case MU mostly satisfies the individual QoS constraints, with values exceeding 1 bps/Hz, except in the case of P_0^{max}=43dBm. In the **ERP**, the worst-case MU throughput is nearly zero.

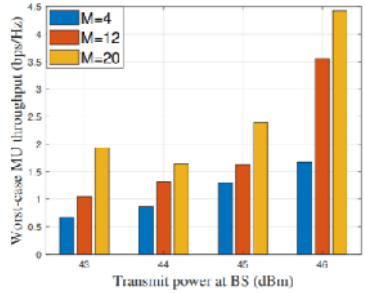

Figure 3. 8 Worst-Case Throughput with $M = 4, M = 12, M = 20$.

Figure 3.8 shows the worst-case MU throughput with respect to the number of RIS (M = 4, M = 12, M = 20), N=200, and K=30. The MU throughput of the proposed method is always greater than 1 bps/Hz. The MU throughput at M=20 is approximately 2.5 times higher than the MU throughput at M=12.

3.4 Chapter Conclusion

First, a cellular mobile network model is proposed with the support of an RIS. In this model, the cellular network supports multiple users divided into different groups at various locations. Second, the wave propagation model for the network is analyzed under the assumption that user groups are obstructed by

obstacles such as buildings. Third, a power control coefficient optimization problem at the base station is proposed and solved based on a power allocation method, with constraints including the maximum total transmit power at the BS and the QoS requirements for each user in each group. Fourth, an optimization problem for the phase shift coefficients of the reflecting elements in the RIS is developed and proposed. The optimization constraints are based on the maximum transmit power of the BS and the phase shift conditions of RIS. Fifth, the optimization problem of the transmit power at the BS is combined with the optimization of the phase shift coefficients of the reflecting elements on the RIS

CHAPTER 4 OPTIMIZATION OF POWER ALLOCATION AND COMPUTATIONAL OFFLOADING IN MEC SYSTEMS WITH UAV-RIS

This chapter focuses on examining the application of the RIS in MEC systems with the support of UAVs. Specifically, the problem of optimizing the power allocation of the MBS and offloading the computation of devices within the system is addressed, with constraints on the computational resources of the devices and QoS. Additionally, the optimization of the UAV's trajectory is considered, aiming to find the shortest and most energy-efficient flight path for the UAV carrying the RIS.

4.1 MEC System Model with UAV-RIS Integration

4.1.1 Proposed System Model

Figure 4.1, the MBS is equipped with a multi-antenna array to communicate with K single-antenna users. It is assumed that all users are divided into M different groups, as denoted below $\mathcal{K}_{\mathcal{U}} = \{\mathcal{K}_1, \dots, \mathcal{K}_{\mathcal{M}}\}$ với $\mathcal{K}_m = \{1, \dots, K_m\}, m = 1, \dots, M$.

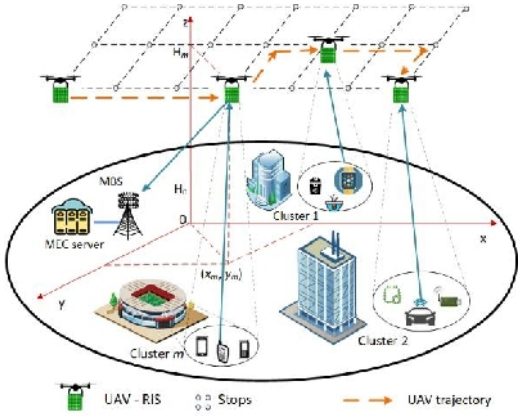

UAV-RIS (RIS: N independent reflecting elements) acts as a relay station serving a small-cell. The model consists of a group of users, denoted as $\mathcal{K}_0$, directly connected to the MBS, while the remaining groups receive support from UAV-RIS. The user (m, k)th corresponds to the kth user in the mth group, with $m =$

Figure 4. 1 Proposed Model Combining UAV $1, \dots, M$ and $k \in \mathcal{K}_m$. and RIS in the MEC System

$u_{m,k}$ is used to determine whether it is necessary to offload the computational task of the kth user in the mth group to the MEC server, as shown in (4.1).

$$u_{m,k} = \begin{cases} 1 & task\ offloading \\ 0 & others \end{cases} \quad (4.1)$$

$u_m = [u_{m,k}]_{k=1}^{K_m}$ và $u = [u_m]_{m=0}^{M}$ represent the user associations.

4.1.2 Channel Model

Assume that the MBS is positioned in a 3D coordinate system xyz, RIS. The RIS and the user are located at $(x_0, y_0, H_0), (x_m, y_m, H_m), m \in \mathcal{M}$, and $(x_k, y_k, 0), k = 1,2, \dots, K$. The antenna heights of the MBS and the RIS are H_0 and H_m, respectively. These coordinates are determined using GPS and are stored in the MBS. The path loss between the MBS and the RIS at the mth position is given by [63]:

$$\beta_{m,0} = \frac{\beta_0}{d_{m,0}^2 + (H_0 - H_m)^2},\ m = 1, \dots, M, \quad (4.2)$$

β_0 is the power gain of the communication channel at d_0 and $d_{m,0} = \sqrt{(x_0 - x_m)^2 + (y_0 - y_m)^2}$.

The path loss expression between the (m,k)th and UAV $(m = 1, \dots, M, k = 1, \dots, K_m)$ is given as [65]:

$$\beta_{m,k} = PL_{m,k} + \eta_{LoS} P_{m,k}^{LoS} + \eta_{NLoS} P_{m,k}^{NLoS}, \quad (4.3)$$

In (4.3), LoS refers to the line-of-sight (LoS) transmission between the MBS and the RIS, while NLoS refers to the obstructed transmission. The coefficients η_{LoS}, η_{NLoS} represent the average path loss factors for LoS and NLoS transmissions, respectively. The path loss coefficient as a function of distance is calculated as follows:

$$PL_{m,k} = 10 \log \left(\frac{4\pi f_c D_{m,k}}{c} \right)^{\alpha}, \quad (4.4)$$

f_c is the carrier frequency (Hz), c is the speed of light (m/s), and the path loss exponent $\alpha \geq 2$, $D_{m,k} = \sqrt{d_{m,k}^2 + H_m^2}$ is the Euclidean distance between the UAV-RIS and the $(m,k)th$ user. The probability of LoS is calculated as follows [66]:

$$P_{m,k}^{LoS} = \frac{1}{1 + a \exp\left[-b\left(\arctan\left(\frac{H_m}{d_{m,k}}\right) - a\right)\right]} \quad (4.5)$$

a và b are environment-dependent constants, and $P_{m,k}^{NLoS} = 1 - P_{m,k}^{LoS}$. For users receiving the direct signal from the MBS, the channel matrix from the $(0,k)$th

user to the MBS is calculated as follows: $G_{k,0} = \sqrt{\beta_{k,0} h_{k,0}} \in C^{L\times 1}$, wherein $\boldsymbol{h}_{k,0}$ are the small-scale fading coefficients. For users that require the assistance of the RIS to ensure communication to the MBS, the channel between the(m,k)th user to the UAV-RIS and from the UAV-RIS to the MBS are represented as $\boldsymbol{h}_{m,k} \in C^{N\times 1}$ and $\boldsymbol{h}_{m,0}^{H} \in C^{L\times N}$ respectively, with $(m \in \mathcal{M}, k \in \mathcal{K}_m)$. Assuming the random variables are i.i.d with zero mean and unit variance, the channel matrices from the (m,k)th to the UAV-RIS and from the UAV-RIS to the MBS are represented as $\boldsymbol{H}_{m,k} \in C^{N\times 1}$ and $\boldsymbol{H}_{m,0}^{H} \in C^{L\times N}$ whrein $\boldsymbol{H}_{m,k} = \sqrt{\beta_{m,k}} h_{m,k}$ và $\boldsymbol{H}_{m,0}^{H} = \sqrt{\beta_{m,0}} h_{m,0}^{H}$. The channel matrix from the (m,k)th user to the MBS, $\boldsymbol{G}_{m,k} \in C^{L\times 1}$ is given by [68]:

$$\boldsymbol{G}_{m,k} = \boldsymbol{H}_{m,0}^{H} \boldsymbol{\Phi}_m \boldsymbol{H}_{m,k}, \qquad m \in \mathcal{M}, \tag{4.6}$$

where $\boldsymbol{\Phi}_m = diag[\phi_{1m}, \phi_{2m}, \dots, \phi_{Nm}]$ is the phase-shifting matrix at the UAV-RIS, $\phi_{nm} = \alpha_{nm} e^{j\theta_{nm}}$, $\alpha_{nm} \in [0,1]$ and $\theta_{nm} \in [0,2\pi]$ for all $(\forall n = 1,2,\dots,N, m \in \mathcal{M})$ representing the amplitude and phase shift coefficient of the nth. reflecting element. Assuming that only the phase component of the signal changes during the reflection process, we have $\alpha_{nm} = 1$ [90].

4.1.3 Received Signal Model and System Throughput

When the (m,k)th user in the mth group requires offloading to the MBS, the signal can be transmitted directly to the MBS or through the UAV-assisted RIS. The received signal at the MBS from the (m,k)th user is given by:

$$y_{m,k} = \sqrt{P_{m,k}} \boldsymbol{G}_{m,k}^{H} \boldsymbol{f}_{m,k} s_{m,k} + \underbrace{\sum_{l=1, l\neq k}^{K_m} \sqrt{P_{l,m}}\, \boldsymbol{G}_{l,m}^{H} \boldsymbol{f}_{l,m} s_{l,m}}_{\text{intra-cell interference}} + n_0, \tag{4.7}$$

In (4.7), $P_{m,k}$ is the transmit power of the (m,k)th, $\boldsymbol{f}_{m,k} \in \mathbb{C}^{L\times 1}$ là is the beamforming vector at the MBS for the (m,k)th user, $s_{m,k}$ s the offloaded data transmitted by the user with (m,k)th with $\left|\left|s_{m,k}\right|\right|^2 \leq 1$, and $n_0 \sim \mathcal{CN}(0, \sigma_0^2)$ is AWGN at the MBS. To suppress intra-cell interference in expression (4.7), the Zero-Forcing (ZF) technique is applied [91]. Let $\boldsymbol{G}_m = \left[G_{m,1}, \dots, G_{m,K_m}\right] \in \mathbb{C}^{L\times K_m} (m = 0,1,\dots,M)$.

Based on large-scale MIMO system assumptions, the ZF-based beamforming matrix is computed as follows:

$$\bar{\boldsymbol{f}}_m = \boldsymbol{G}_m (\boldsymbol{G}_m^{H} \boldsymbol{G}_m)^{-1}, \tag{4.8}$$

where $\bar{\boldsymbol{f}}_m = \left[\bar{\boldsymbol{f}}_{m,1}, \dots, \bar{\boldsymbol{f}}_{m,K_m}\right] \in \mathbb{C}^{L\times K_m}$, $\bar{\boldsymbol{f}}_{m,k} \in \mathbb{C}^{L\times 1}$, $m = 0,1,\dots,M, k \in K_m$. The normalized beamforming vector is then given by:$\tilde{\boldsymbol{f}}_{m,k} = \bar{\boldsymbol{f}}_{m,k} / \left\|\bar{\boldsymbol{f}}_{m,k}\right\|$ and and the final beamforming vector $\boldsymbol{f}_{m,k}$ is expressed as:

$$\boldsymbol{f}_{m,k} = \sqrt{p_{m,k}}\tilde{\boldsymbol{f}}_{m,k}, m = 0,1,\dots,M, k \in \mathcal{K}_m, \quad (4.9)$$

In (4.9), $p_{m,k}$ is the power control coefficient for the (m,k)th user. Substituting into (4.7), the received signal at the MBS becomes:

$$y_{m,k} = \sqrt{P_{m,k}}\sqrt{p_{m,k}}G_{m,k}^H\tilde{\boldsymbol{f}}_{m,k}s_{m,k} + n_0, \quad (4.10)$$

The power control vectors are denoted as $p_m = \left[p_{m,k}\right]_{k=1}^{K_m}$, $\boldsymbol{p} = [p_m]_{m=0}^{M}$, và $\boldsymbol{\Phi} = [\boldsymbol{\Phi}_m]_{m=1}^{M}$the phase shift matrices of the RIS. The achievable throughput (in bits per second) at the MBS is given by:

$$R_{m,k}(p_{m,k}, \boldsymbol{\Phi}_m) = W\log_2\left(1 + \frac{P_{m,k}p_{m,k}\left|\boldsymbol{G}_{m,k}^H\tilde{\boldsymbol{f}}_{m,k}\right|^2}{\sigma_0^2}\right), \quad (4.11)$$

where W denotes the bandwidth allocated to the(m,k)th user.

4.1.4 Task Offloading Model

Let $\mathcal{I}_{m,k}$ (bits) denote the size of the computational task to be offloaded, and let $\mathcal{F}_{m,k}$ represent the number of CPU cycles required to compute one bit of the task $\mathcal{I}_{m,k}$. The local and offloading latency associated with processing the task for the $\mathcal{I}_{m,k}$ user is defined as follows:

4.1.4.1 Local Computation

Let $c_{m,k}$ denote the computing capacity of the (m,k)th user. If the user executes the computation locally, the computation latency is given by:

$$T_{m,k}^l = \frac{\mathcal{I}_{m,k}\mathcal{F}_{m,k}}{c_{m,k}}, m = 0,1,\dots,M, k \in K_m. \quad (4.12)$$

4.1.4.2 Task Offloading to the MBS

The transmission time required to offload the task from the (m,k)th user $(m = 0,1,\dots,M, k \in \mathcal{K}_m)$ to the MBS is given by:

$$T_{m,k}^{tx}(p_{m,k}, \boldsymbol{\Phi}_m) = \frac{\mathcal{I}_{m,k}}{R_{m,k}(p_{m,k}, \boldsymbol{\Phi}_m)}, \quad (4.13)$$

The computation time at the MBS for the offloaded task is expressed as:

$$T_{m,k}^{com}(\zeta_{m,k}^{bs}) = \frac{\mathcal{I}_{m,k}\mathcal{F}_{m,k}}{\zeta_{m,k}^{bs}}, m = 0,1,\dots,M, k \in K_m, \quad (4.14)$$

where $\zeta_{m,k}^{bs}$ denotes the computation resource allocated by the MBS for processing the task of the (m,k)th user. For simplicity, we define $\zeta_m = \left[\zeta_{m,k}^{bs}\right]_{k=1}^{K_m}$, and $\zeta = [\zeta_m]_{m=0}^{M}$ representing the overall allocation of computational resources at the MBS. From equations (4.12) - (4.14), the total latency for executing the task of the (m,k)th user can be derived accordingly.

$$\begin{aligned} T_{m,k}^{tot}(p_{m,k}, u_{m,k}, \boldsymbol{\Phi}_m, \zeta_{m,k}^{bs}) &= (1 - u_{m,k})T_{m,k}^l \\ &+ u_{m,k}\left(T_{m,k}^{tx}(p_{m,k}, \boldsymbol{\Phi}_m) + T_{m,k}^{com}(\zeta_{m,k}^{bs})\right). \end{aligned} \quad (4.15)$$

The time required to transmit the computation results from the MBS back to the user can be neglected, as it is negligible compared to the total task execution time [79], [92].

4.1.5 UAV Trajectory

Table 4. 1: Shortest Flight Path of the UAV

Algo 1: The shortest path finding	Assume that the UAV flight through $\boldsymbol{M}$ stop points, each corresponding to one of the $\boldsymbol{M}$ user groups requiring computation offloading. These points are located on a 2D rectangular grid at a fixed altitude $\boldsymbol{H_m}$. Algo 1 aims to determine the UAV's flight trajectory through fixed stop point positions, with the initial position $(\mathbf{0}, \mathbf{0}, \boldsymbol{H_m})$, $(\boldsymbol{x_m}, \boldsymbol{y_m}, \boldsymbol{H_m})$ is the final stop point with fixed coordinates and altitude, $\boldsymbol{d}_{\max}$ is the maximum allowable travel distance for the UAV $\boldsymbol{\mathcal{T}}$.

Requirements: $(0,0,H_m)$, (x_m, y_m, H_m), $d_{\max}$
Constraint: $\mathcal{T}$
Stop points of UAV.
for $\mathcal{R}$ in $\mathcal{M}$
Compute the distance d from UAV to the final stop point
if $d < d_{\max}$ **then**
$\mathcal{T} \leftarrow \mathcal{R}$
$d_{\max} = d$
end if
end for	

4.2 Latency Optimization Based on Resource Allocation and Computation Offloading

The problem considers a joint optimization framework that includes user power allocation $(\boldsymbol{p})$, user association (u), phase shift configuration of the RIS $(\boldsymbol{\Phi})$, and computation resource allocation at the MBS (ζ). The objective is to minimize the total system latency, subject to constraints on computational resources and QoS requirements.

$$\min_{\boldsymbol{p},u,\boldsymbol{\Phi},\zeta} \sum_{m=0}^{M} \sum_{k=1}^{K_m} T_{m,k}^{tot}\left(p_{m,k}, u_{m,k}, \boldsymbol{\Phi}_m, \zeta_{m,k}^{bs}\right) \tag{4.16a}$$

$$\text{s.t} \quad 0 \le p_{m,k} \le 1, \tag{4.16b}$$

$$R_{m,k}\left(p_{m,k}, \Phi_m\right) \ge \bar{r}_0, m = 0,1,\dots,M, k \in K_m, \tag{4.16c}$$

$$0 \le \theta_{nm} \le 2\pi, \forall n = 1,2,\dots,N, m \in M, \tag{4.16d}$$

$$\sum_{k=1}^{K_m} u_{m,k}\zeta_{m,k}^{bs} \le \zeta_{max}, \tag{4.16e}$$

4.2.1 Power Allocation Optimization

Given fixed values of $\boldsymbol{\Phi}$, u, ζ expression (4.16) can be rewritten as follows:

$$\min_{p} \sum_{m=0}^{M} \sum_{k=1}^{K_m} T_{m,k}^{tot}\left(p_{m,k}\right) \tag{4.17a}$$

$$s.t \quad \text{(4.16b), (4.16c)} \tag{4.17b}$$

The optimization problem in expression (4.17) can be solved by leveraging the following convex function: $f(x) = \log_2\left(1+\frac{1}{x}\right)$ with $x > 0$

$$f(x) = \log_2\left(1+\frac{1}{x}\right) \geq \hat{f}(x), \tag{4.18}$$

For $\forall x > 0, \bar{x} > 0$, we have:

$$\begin{aligned}\hat{f}(x) = & \log_2\left(1+\frac{1}{\bar{x}}\right) + \left(\frac{\partial f(\bar{x})}{\partial x}\right)(x-\bar{x}) \\ = & \log_2\left(1+\frac{1}{\bar{x}}\right) + \frac{1}{1+\bar{x}} - \frac{x}{(1+\bar{x})\bar{x}}\end{aligned} \tag{4.19}$$

The throughput at the MBS to transmit information to the user $(m,k)th$ in equation (4.11) is as follows:

$$R_{m,k}(p_{m,k}) \geq \hat{R}^{(i)}_{m,k}(p_{m,k}),\ \forall m \in \mathcal{M},\ \forall k \in \mathcal{K}_m, \tag{4.20}$$

$$\hat{R}^{(i)}_{m,k}(p_{m,k}) = W\left(\log_2\left(1+\frac{1}{\bar{x}}\right) + \frac{1}{1+\bar{x}} - \frac{x}{(1+\bar{x})\bar{x}}\right). \tag{4.21}$$

Let $\boldsymbol{r} \triangleq \{r_{m,k}\}$ $(\forall m \in \mathcal{M}, \forall k \in \mathcal{K})$ satisfy the condition: $\frac{1}{R_{m,k}(p_{m,k})} \leq r_{m,k}$.

$$\begin{aligned}T^{tot}_{m,k}(r_{m,k}) &\leq \hat{T}^{tot}_{m,k}(r_{m,k}) \\ &= (1-u_{m,k})T^{l}_{m,k} + u_{m,k}(r_{m,k}\mathcal{I}_{m,k} + T^{com}_{m,k}).\end{aligned} \tag{4.22}$$

We can then rewrite the optimization problem in expression (4.17) as:

$$\min_{p,r} \sum_{m=0}^{M}\sum_{k=1}^{K_m} \widehat{T^{tot}_{m,k}}(r_{m,k}) \tag{4.23a}$$

$$s.t \quad p_{m,k} \leq 1, P_{m,k} \leq P^{max} \tag{4.23b}$$

$$\widehat{R^{(i)}_{m,k}}(p_{m,k}) \geq \bar{r}_0, \tag{4.23c}$$

$$\frac{1}{\widehat{R^{(i)}_{m,k}}} \leq r_{m,k}, m = 0,1,\dots,M, k \in \mathcal{K}_m, \tag{4.23d}$$

Table 4. 2: Power Allocation Optimization

Algorithm 2: Optimal Power Allocation

Input: u, $\boldsymbol{\Phi}$, ζ, and initialization $p^{(0)}$, $\varepsilon = 10^{-3}$, $I_{max} = 20$

for $m = 1$ to M

$$i = 0$$

repeat

Solve (4.23) to find $\boldsymbol{p}^{(i+1)}$; $i = i+1$

until convergence or $i > I_{max}$;

end for

Output: $\boldsymbol{p}^*$

The problem (4.23) is a standard convex optimization problem, which can be solved using the CVX tool [70] as shown in Algo 2.

4.2.2 Optimal Phase Shift Coefficient

With fixed values of $\boldsymbol{p}$, $\boldsymbol{u}$, ζ expression (4.16) can be rewritten as follows:

$$\min_{\boldsymbol{\Phi}} \sum_{m=0}^{M} \sum_{k=1}^{K_m} T_{m,k}^{tot}(\boldsymbol{\Phi}_m) \tag{4.24a}$$

$$\text{s.t} \quad (4.16c), (4.16d) \tag{4.24b}$$

With a fixed beamforming vector at the transmitter side $\left(\boldsymbol{f}_{m,k}, \forall n = 1,2,\dots,N, m \in \mathcal{M}\right)$, define the phase shift vector $\nu_m = [\nu_m^1, \dots, \nu_m^N]^H$, where $\nu_m^n = e^{j\theta_{nm}}, (\forall n = 1,2,\dots,N)$. The constraint in (4.16d) is as follows: $|\nu_m^n|^2 = 1$. Define $\chi_{m,k} = diag\left(\boldsymbol{H}_{m,0}^H\right)\boldsymbol{H}_{m,k}\tilde{\boldsymbol{f}}_{m,k}$, $H_{m,0}^H \boldsymbol{\Phi}_m H_{m,k}\tilde{\boldsymbol{f}}_{m,k} = \nu_m^H \chi_{m,k}$ We can apply the approximation (4.20) - (4.21) as follows:

$$R_{m,k}(\boldsymbol{\Phi}_m) \geq \tilde{R}_{m,k}^{(i)}(\boldsymbol{\Phi}_m), \ \forall m \in \mathcal{M}, \ \forall k \in \mathcal{K}_m, \tag{4.25}$$

$$\tilde{R}_{m,k}^{(i)}(\boldsymbol{\Phi}_m) = W\left(\log_2\left(1 + \frac{1}{\bar{y}}\right) + \frac{1}{1+\bar{y}} - \frac{y}{(1+\bar{y})\bar{y}}\right), \tag{4.26}$$

Define the variable $\tilde{r} \triangleq \{\tilde{r}_{m,k}\}$ $(\forall m \in \mathcal{M}, \forall k \in \mathcal{K})$ $\frac{1}{R_{m,k}(\boldsymbol{\Phi}_m)} \leq \tilde{r}_{m,k}$

$$\begin{aligned} T_{m,k}^{tot}\left(\tilde{r}_{m,k}\right) &\leq \tilde{T}_{m,k}^{tot}\left(\tilde{r}_{m,k}\right) \\ &= \left(1 - u_{m,k}\right)T_{m,k}^{l} + u_{m,k}\left(\tilde{r}_{m,k}\mathcal{I}_{m,k} + T_{m,k}^{com}\right). \end{aligned} \tag{4.27}$$

Thus, expression (4.24) can be equivalently rewritten as:

$$\min_{\nu_m, \tilde{r}, m \in \mathcal{M}} \sum_{m=0}^{M} \sum_{k=1}^{K_m} \tilde{T}_{m,k}^{tot}\left(\tilde{r}_{m,k}\right) \tag{4.28a}$$

$$\text{s.t} \quad \nu_m^H \chi_{m,k} \chi_{m,k}^H \nu_m \geq (2^{\overline{r_0}} - 1)/a_k, m \in \mathcal{M}, k \in \mathcal{K}_m, \tag{4.28b}$$

$$|\nu_m^n|^2 = 1, \forall n = 1,2,\dots,N, m \in \mathcal{M}, \tag{4.28c}$$

$$\frac{1}{\tilde{R}_{m,k}^{(i)}} \leq \tilde{r}_{m,k}, \qquad m = 0,1,\dots,M, \qquad k \in \mathcal{K}_m \tag{4.28d}$$

The constraint in (4.28b) is equivalent to (4.16c), with $a_k = P_{m,k}p_{m,k}/\sigma_0^2$. Expression (4.28) is a non-convex QCQP, which cannot be solved directly using the CVX library. We need to reformulate the problem, introducing $\boldsymbol{X}_{m,k} = \chi_{m,k}\chi_{m,k}^H$ và $\nu_m^H \boldsymbol{X}_{m,k} \nu_m = tr\left(\boldsymbol{X}_{m,k}\nu_m\nu_m^H\right) = tr\left(\boldsymbol{X}_{m,k}V_m\right)$, với $V_m = \nu_m\nu_m^H$ must satisfy $\mathrm{V_m} \succeq 0$ and $rank(V_m) = 1$ [46] [49]. Therefore, expression (4.28) is transformed into:

$$\min_{\nu_m, \tilde{r}, m \in \mathcal{M}} \sum_{m=0}^{M} \sum_{k=1}^{K_m} \tilde{T}_{m,k}^{tot}\left(\tilde{r}_{m,k}\right) \tag{4.29a}$$

$$\text{s.t} \qquad \mathrm{tr}\left(\mathbf{X}_{\mathrm{m,k}}\mathbf{V}_{\mathrm{m}}\right) \geq (2^{\overline{\mathrm{r_0}}} - 1)/\mathrm{a_k}, \qquad \mathrm{m} \in \mathcal{M}, \mathrm{k} \in \mathcal{K}_m, \tag{4.29b}$$

$$\mathbf{V}_{\mathrm{m}(n,n)} = 1, \forall n = 1,2,\dots,N, m \in \mathcal{M}, \tag{4.29c}$$

$$\mathbf{V}_{\mathrm{m}} \succeq 0 \tag{4.29d}$$

$$\frac{1}{\tilde{R}_{m,k}^{(i)}} \leq \tilde{r}_{m,k}, \qquad m = 0,1,\dots,M, \qquad k \in \mathcal{K}_m \tag{4.29e}$$

Table 4. 3: Optimal Phase Shift Coefficient

Algorithm 3: Finding optimal phase

Input: u, ζ, $\boldsymbol{p}$, and initial $f_{m,k}^{(0)}$

Constraints: $f_{m,k}^{(0)}$, $\varepsilon = 10^{-3}$, $I_{max} = 20$

for $m = 1$ to M

$i = 0$

repeat

Solve the problem (4.29) to find $\boldsymbol{\Phi}_m^{(i+1)}$

$f_{m,k}^{(i+1)}$, $i = i + 1$

until convergence or $i > I_{max}$

end for

Output: $\boldsymbol{\Phi}_{\boldsymbol{M}}^{*}$

Given $y = \frac{\sigma_0^2}{P_{m,k} p_{m,k} tr(\mathrm{X}_{m,k} \boldsymbol{V}_m)}$. expression (4.29) is an SDP problem [41][46], and this problem can be solved using the CVX tool. The BCD method is proposed for solving the problem in expression (4.29).

4.2.3 Computation Offloading Optimization

With fixed values of $\boldsymbol{p}$, u, $\boldsymbol{\Phi}$, expression (4.16) can be rewritten as:

$$\min_{\zeta} \sum_{m=0}^{M} \sum_{k=1}^{K_m} T_{m,k}^{tot}\left(\zeta_{m,k}^{bs}\right) \tag{4.30a}$$

s.t (4.16e) (4.30b)

Table 4.4 Iterative Optimization Algorithm

Algorithm 4: Iterative Optimization Algorithm for Solving (4.16)

Input: u, $\boldsymbol{\Phi}$, $\boldsymbol{\zeta}$ and initial $\boldsymbol{p}^{(0)}$, $f_{m,k}^{(0)}$, $\zeta^{(0)}$

Constraints:

$\varepsilon = 10^{-3}$, $I_{max} = 20$, $j = 0$

repeat

Solve (4.23), for feasible $\boldsymbol{p}^{(j+1)}$

Solve (4.29), for feasible $\boldsymbol{f}_{m,k}^{(i+1)}$

Solve (4.30), for feasible $\boldsymbol{\zeta}^{(j+1)}$

$j = j + 1$

until Convergence or $j > I_{max}$

Output: $\boldsymbol{p}^{*}$, $\boldsymbol{f}_{\boldsymbol{m,k}}^{*}$, $\boldsymbol{\zeta}^{*}$

Since the objective function and the constraint in expression (4.16e) are convex with respect to $\boldsymbol{\zeta}$, problem (4.30) can be solved using the CVX library. Finally, an iterative optimization algorithm is proposed to simultaneously determine the optimal power allocation, find the phase shift coefficients, and perform computation offloading optimization. In Algo 4, the optimization result from each iteration is used as the starting point for the next iteration.

4.3 Convergence Analysis and Computational Complexity of the Proposed Method

For problem (4.16), an alternating optimization approach is employed, iteratively solving subproblems for power allocation (4.23) using a convex approximation of (4.18)-(4.21), RIS configuration (4.29) transformed from QCQP (4.24) to SDP with $\boldsymbol{V_m} = \nu_m \nu_m^H$, and MEC allocation (4.30). The algorithm terminates when the objective function change is less than $\varepsilon = 10^{-3}$, or $I_{max} = 20$. Due to the successive convex approximation (SCA) in (4.23) and the monotonic decrease of the objective function $\boldsymbol{\mathcal{F}}(\boldsymbol{p}, \boldsymbol{\Phi}, \boldsymbol{\zeta})$, the sequence $\boldsymbol{\mathcal{F}}(\boldsymbol{p}^{(i)}, \boldsymbol{\Phi}^{(i)}, \boldsymbol{\zeta}^{(i)}$ converges to a stationary point of the relaxed problem with $rank(\boldsymbol{V_m}) = 1$ [111].

With M user groups, K users per group, and N RIS reflecting elements, the power allocation subproblem (4.23) has $\mathcal{O}(MK)$ variables with a complexity of $\tilde{\mathcal{O}}((MK))^3$, while the RIS subproblem (4.29) involves $\mathcal{O}(N^2)$ variables with a complexity of $\tilde{\mathcal{O}}(MKN^6)$. The MEC subproblem (4.30) has a complexity of $\tilde{\mathcal{O}}((MK)^3)$. The total computational cost per iteration is $\tilde{\mathcal{O}}(MKN^6)$, leading to an overall complexity of $\tilde{\mathcal{O}}(I.MKN^6)$ for $I \leq I_{max} = 20$) iterations[84, 112].

4.4 Simulation Results

The simulation is carried out in MATLAB using the CVX tool, with simulation parameters configured as shown in Table 4.4. The objective of the simulation results is to compare the proposed optimization method with non-optimized cases such as:

• Network total latency minimization, defined as $\sum_{m=0}^{M} \sum_{k=1}^{K_m} T_{m,k}^{tot}$.

• Worst-case total latency minimization, defined as: $\sum_{m=0}^{M} \max_{k \in \mathcal{K}_m} \{T_{m,k}^{tot}\}$

Table 4. 4: Simulation Parameters

No.	Parameter	Value
1	Number of MBSs	1
2	Near coverage radius	500m
3	Far coverage radius	2000m
4	Location of MBS	(0,0,30)
5	UAV altitude range$\left(H^{min}, H^{max}\right)$	$(50,150)m$
6	Carrier frequency	2.4GHz
7	Channel bandwidth	1 MHz
8	Channel bandwidth $P_{m,k}$	30 dBm
9	QoS threshold	$\bar{r_0} = 1$ Mbps
10	Power spectral density of white	$\sigma^2 = -130\, dBm/Hz$

	Gaussian noise	
11	Size of offloaded task [93]	$D_m = 100\ kB$
12	Task complexity [93]	$\mathcal{F}_{m,k} = 600\ cycles/bit$
13	Maximum computing resource [93]	$\zeta_{max} = 30\ \ Giga\ cycles/s$
14	Maximum computing capability [93]	$c_{m,k} = 0.5\ \ Giga\ cycles/s$

4.4.1 Convergence Analysis

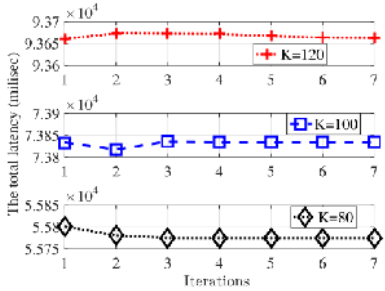

Figure 4. 2 The convergence of the proposed approach

Figure 4.2 illustrates that the proposed method requires a few iterations to solve the optimization problem based on Algo 4. Specifically, when K = 80 or K = 100, the algorithm converges after 3 iterations, while more iterations are needed when K = 120. This is because increasing the number of users corresponds to an increase in the number of optimization variables.

4.4.2Total latency of UE users in the system under varying computational complexity $\mathcal{F}_{m,k}$

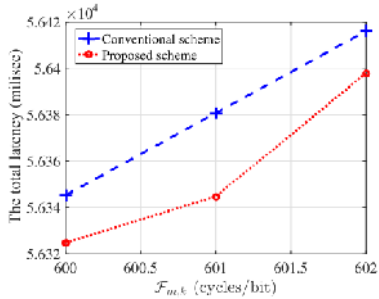

(a) N =80

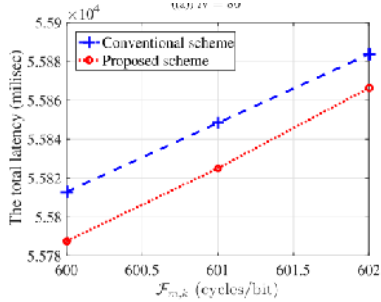

(b) N = 100

Figure 4. 3: Total network latency with different resource allocation schemes $\mathcal{F}_{m,k}$, with $K = 80, \zeta_{max} = 30\ Giga\ cycles/s$.

Figures 4.3(a) and 4.3(b) compare the total latency with N = 80 and $\mathcal{F}_{m,k} = 600$. The total latency of the proposed method is $5.632x10^4 ms$. As the number of reflecting elements increases, the total network latency decreases [44].

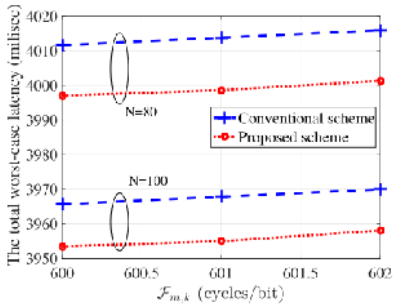

Figure 4. 4: The Total worst-case latency with different resource allocation schemes ζ_{max}, with $K = 80, \mathcal{F}_{m,k} = 600\ cycles/bit$.

In Figure 4.4, the total latency is evaluated in the worst-case scenario with different values of CPU cycles, $\mathcal{F}_{m,k}$. From the simulation results, it is observed that the total latency increases with the number of CPU cycles required to compute each bit of the task, i.e., the computational complexity of the task. Therefore, the UEs (User Equipments) need to offload their local computation to the MEC server to reduce the latency.

4.4.3 Total Latency of Users with Maximum Computation Resources of MEC server ζ_{max}.

In Figure 4.5, the total network latency is compared with other methods within a computational capability range of the MBS (*Mega cycles/s*), ζ_{max}. The number of users and CPU cycles are set to K = 80 and $\mathcal{F}_{m,k} = 600\ cycles/bit$, respectively. The results show that as the number of RIS elements and the computational capability of the MBS increase, the total network latency significantly decreases when the computational capability of the MBS is enhanced.

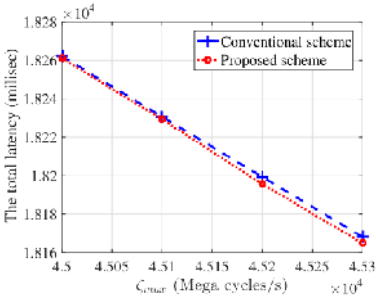

(a) N = 80

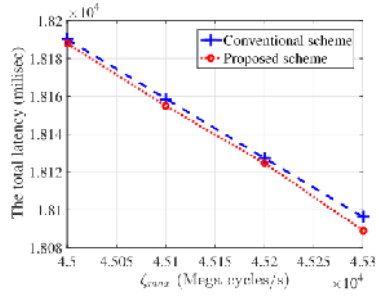

(b) N =100

Figure 4. 5 The total network latency with different resource allocation schemes varying ζ_{max}, $K = 80, \mathcal{F}_{m,k} = 600\ cycles/bit$

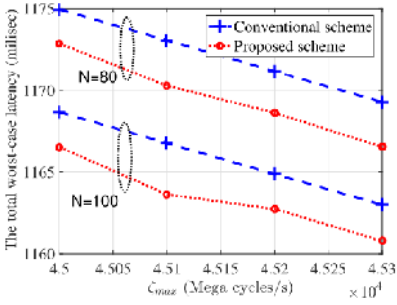

In Figure 4.6, the advantages of the proposed method for the UAV-RIS supported MEC system are demonstrated in terms of the total latency in the worst-case scenario. It can be observed that the total latency in the worst-case scenario significantly decreases as the computational capability increases.

Figure 4. 6 The worst-case latency with $K = 80, \mathcal{F}_{m,k} = 600\ cycles/bit$ and varying ζ_{max}.

4.5 Conclusion

In summary, the simulation results of the proposed algorithm for optimizing resource allocation and offloading computation for the MEC system supported by UAV-RIS outperform the case where the transmission power is the same and the phase angle of the intelligent reflecting surface is random. However, the simulation results in Figures 4.2a and 4.3a, when considering the total latency of all users in the network compared to the computation complexity and the maximum computational resources of the server, do not yet show the superiority of the proposed optimization algorithm.

CHAPTER 5 CONCLUSION

5.1 Conclusion

This dissertation focuses on exploring the application of RIS in wireless communication networks, specifically in cellular networks and MEC systems supported by UAV-RIS. The dissertation has successfully achieved the objectives outlined in the overview with the following key results:

First, the dissertation considers a wireless communication model supported by RIS, where multiple RIS devices are deployed to assist the downlink for different groups of users. For the proposed model, the optimization problem is formulated with the goal of maximizing the total network throughput, subject to constraints on the power consumption at the base station and the QoS. Since the proposed problem is non-convex, the initial optimization problem is divided into two subproblems. The first problem involves power control with fixed phase shift values. In this case, the problem is convex, making it easier to find a solution using supporting tools. Subsequently, a method for phase shift coefficient search is proposed to solve the non-convex problem and determine the optimal phase shift coefficients of the reflecting elements.

Secondly, the dissertation proposes an optimization problem for the MEC system, situated within a large-scale MBS, supported by UAVs carrying RIS that are capable of flying within the network coverage area. The optimization problem aims to minimize the total latency of the proposed system by optimizing the power allocation for each user, user-linking, phase shift configuration of the RIS elements, and computational resource allocation at the MBS, subject to computational resource constraints and the QoS requirements of the MBS. To solve this problem, an iterative algorithm has been designed to efficiently solve the proposed optimization problem by applying several approximation methods and inequalities, following the movement path and BCD method. In addition, the dissertation also proposes a method to determine the UAV's flight trajectory based on the user density on the ground.

Indeed, RIS, with its numerous advantages, is considered one of the key technologies for 6G communication. Specifically, 6G networks promise to deliver various services in the future with stringent requirements for extremely high data transmission speeds of up to 100 Gbps, ultra-low latency below 1 ms, and high user density. The application of RIS in 6G networks helps enhance signal strength and coverage due to its ability to adjust radio waves, improving connection quality, reducing interference, and saving energy compared to traditional transmission solutions.

5.2 Future Directions

In the first research problem, the case where the BS is equipped with multiple antennas has not been considered. Additionally, the optimal number of elements has not been addressed. The problem of continuous energy and information transmission has also not been analyzed or evaluated in the system.

In the second research problem, the UAV-RIS is considered for serving specific user groups, assuming the UAV-RIS is stationary. In practice, the issue of UAV instability due to environmental effects should be considered. Specifically, increasing the number of UAVs with the goal of supporting larger-scale services needs to be explored. Furthermore, an important issue is the optimization of the number of user groups and the flight path trajectory, with the goal of minimizing latency and saving energy for the UAV. Additionally, the doctoral candidate is currently researching the application of reinforcement learning and deep reinforcement learning to solve optimization problems.